THE JOURNAL OF BIOLOGICAL CHEMISTRY VOL. 289, NO. 28, pp. 19659–19669, July 11, 2014

Structural and Evolutionary Aspects of Antenna Chromophore Usage by Class II Photolyases*

Received for publication, December 19, 2013, and in revised form, May 4, 2014 Published, JBC Papers in Press, May 21, 2014, DOI 10.1074/jbc.M113.542431

Stephan Kiontke[‡1], **Petra Gnau**[‡], **Reinhard Haselsberger**[§], **Alfred Batschauer**[¶], **and Lars-Oliver Essen**[‡2]

From the [‡]*Biomedical Research Centre/FB15, Unit for Structural Biochemistry, Philipps-University, Hans-Meerwein-Strasse, D-35032 Marburg, Germany, the* [§]*School of Physical and Mathematical Sciences, Division of Physics and Applied Physics, Nanyang Technological University, SPMS-PAP-03-11, 21 Nanyang Link, Singapore 637371, and the* [¶]*Faculty of Biology, Department of Plant Physiology and Photobiology, Philipps-University, Karl-von-Frisch-Strasse 8, D-35032 Marburg, Germany*

Background: Photolyases are light-driven DNA repair enzymes harboring a catalytic FAD cofactor and usually an antenna chromophore.
Results: 8-Hydroxydeazaflavin is the cognate antenna of the *Methanosarcina mazei* photolyase, an archaeal representative of the clade of otherwise metazoan class II photolyases.
Conclusion: Phylogenetically, photolyases lost 8-hydroxydeazaflavin as antenna only in higher plants.
Significance: 8-Hydroxydeazaflavin occurs as cofactor within major parts of the metazoan phylome.

Light-harvesting and resonance energy transfer to the catalytic FAD cofactor are key roles for the antenna chromophores of light-driven DNA photolyases, which remove UV-induced DNA lesions. So far, five chemically diverse chromophores have been described for several photolyases and related cryptochromes, but no correlation between phylogeny and used antenna has been found. Despite a common protein topology, structural analysis of the distantly related class II photolyase from the archaeon *Methanosarcina mazei* (*Mm*CPDII) as well as plantal orthologues indicated several differences in terms of DNA and FAD binding and electron transfer pathways. For *Mm*CPDII we identify 8-hydroxydeazaflavin (8-HDF) as cognate antenna by *in vitro* and *in vivo* reconstitution, whereas the higher plant class II photolyase from *Arabidopsis thaliana* fails to bind any of the known chromophores. According to the 1.9 Å structure of the *Mm*CPDII·8-HDF complex, its antenna binding site differs from other members of the photolyase-cryptochrome superfamily by an antenna loop that changes its conformation by 12 Å upon 8-HDF binding. Additionally, so-called N- and C-motifs contribute as conserved elements to the binding of deprotonated 8-HDF and allow predicting 8-HDF binding for most of the class II photolyases in the whole phylome. The 8-HDF antenna is used throughout the viridiplantae ranging from green microalgae to bryophyta and pteridophyta, *i.e.* mosses and ferns, but interestingly not in higher plants. Overall, we suggest that 8-hydroxydeazaflavin is a crucial factor for the survival of most higher eukaryotes which depend on class II photolyases to struggle with the genotoxic effects of solar UV exposure.

Besides photosynthetic reaction centers and protochlorophyllide reductases DNA photolyases belong to a few light-driven enzymes, which convert light energy into breakage of UV-B-induced bonds between neighboring pyrimidines (1). As highly efficient DNA repair enzymes, photolyases harvest blue/near-UV light photons for channeling excitation energy into the cleavage of non-oxidative photoproduct lesions in DNA. These lesions are caused by solar exposure of non-shielded DNA to UV-B ($\lambda \sim 280–315$ nm) and UV-C ($\lambda \sim 100–280$ nm) and consist for 10–20% of the pyrimidine (6-4)[3] pyrimidone photoproduct, and for 80–90% of the cyclobutane pyrimidine dimer (CPD) lesion in its *cis-syn* isoform (2). Given the predominance and genotoxicity of the latter, most organisms confronted with sunlight, including archaea, bacteria, and eukaryotes, utilize CPD photolyases to maintain their genomic integrity. Only a few evolutionary later evolved organisms such as the placental mammals afford the loss of photolyase orthologues by relying on alternative DNA repair pathways for the maintenance of their genomic integrity (3, 4).

The catalytic mechanism of photolyases generally employs the photo-induced injection of an electron from a fully reduced and typically U-shaped flavin adenine dinucleotide cofactor ($FADH^-$) onto the DNA lesion. This electron transfer triggers cleavage of CPD or (6-4) photoproducts inside duplex DNA (1, 5) within less than a nanosecond and achieves quantum yields close to one for CPD repair (6, 7). Spectroscopic and structural studies (8–10) showed that class I, class II, and (6-4) photolyases catalyze transient electron transfer to these DNA lesions by binding the lesions next to the $FADH^-$ cofactor in the catalytic α-helical C-terminal domain. The N-terminal domain of these photolyases adopts a Rossmann fold, which can accommodate additional prosthetic groups, so called antenna chromophores. Compared with other members of the

* This work was supported by the LOEWE (Landesoffensive zur Entwicklung Wissenschaftlich-Ökonomischer Exzellenz) Center for Synthetic Microbiology (Marburg) and Deutsche Forschungsgemeinschaft Grant BA985/12-1.
The atomic coordinates and structure factors (codes 4CDM and 4CDN) have been deposited in the Protein Data Bank (http://wwpdb.org/).
[1] Present address: Dept. of Biology/Chemistry, Structural Biology, University of Osnabrück, Barbarastr. 13, D-49076 Osnabrück, Germany.
[2] To whom correspondence should be addressed: Biomedical Research Center/FB15, Philipps-University Marburg, Hans-Meerwein-Str., D-35032 Marburg, Germany. Tel.: 4964212822032; Fax: 4964212822191; E-mail: essen@chemie.uni-marburg.de.

[3] The abbreviations used are: (6-4), pyrimidine(6-4)pyrimidone dimer; CPD, cyclobutane pyrimidine dimer; FO synthase,7,8-didemethyl-8-hydroxy-5-deazariboflavin synthase; 8-HDF, 8-hydroxydeazaflavin; *Mm*CPDII, class II CPD-photolyase from *Methanosarcina mazei*; MTHF, 5,10-methenyltetrahydrofolate; PDB, Protein Data Bank.

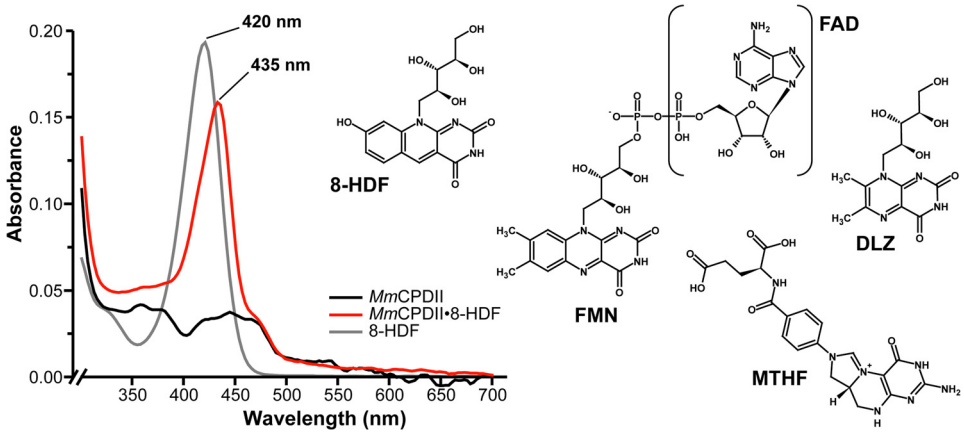

FIGURE 1. ***In vitro* reconstitution of apo*Mm*CPDII with synthetic 8-HDF and overview of known antenna chromophores of members of the photolyase-cryptochrome family.** Binding of 8-HDF to the *M. mazei* class II photolyase (*red curve*) causes a red shift by 15 nm compared with free 8-HDF at pH 8 (*gray curve*), where free 8-HDF is deprotonated at its 8-OH group (pK_a 6.3) like *Mm*CPDII-bound deazaflavin.

photolyase-cryptochrome family, class II photolyases are evolutionary distant with pairwise sequence identities of <16%. Nevertheless, structures of class II photolyases from a methanogenic archaeon (8) as well as from a higher plant (11) indicate a similar bilobal architecture as class I and (6-4) photolyases and cryptochromes. Although class II photolyases catalyze like class I CPD photolyases and DASH cryptochromes light-driven DNA-repair and photoreduction of the catalytic FAD cofactor, they show marked differences for their active site structures, the mode of DNA binding, the electron transfer pathways required for photoreduction as well as for the discrimination between intact and UV lesion-containing DNA.

A shortcoming of the catalytic $FADH^-$ cofactor is its poor absorption in the blue to near-UV range with extinction coefficients between 2800 $M^{-1}cm^{-1}$ (400 nm) and 5600 $M^{-1}cm^{-1}$ (360 nm). For efficient light-driven repair in the blue/near-UV region, photolyases hence rely on a second auxiliary chromophore with large absorption cross-sections to broaden up their limited spectral properties. So far, five different classes of antenna chromophores have been identified from members of the photolyase-cryptochrome superfamily (Fig. 1). These antenna chromophores comprise aromatic moieties absorbing in the range between 380 and 420 nm and include (i) 5,10-methenyltetrahydrofolate (MTHF) as found in many microbial class I photolyases (12) and DASH cryptochromes (13); (ii) 8-hydroxydeazaflavin (8-HDF) from (6-4) photolyases (14, 15) and several class I photolyases (16); (iii and iv) flavin mononucleotide (FMN) and FAD in the class I photolyases from *Thermus thermophilus* (17) and *Sulfolobus tokodaii* (18), respectively; and finally (v) 6,7-dimethyl-8-ribityl-lumazin in a novel class of proteo-/cyanobacterial cryptochromes (19). For light harvesting the antenna chromophores absorb a photon and transfer its energy via a Förster mechanism to the catalytic active $FADH^-$. All nucleotide-like chromophores (FAD, FMN, and 8-HDF) are bound within the N-terminal α/β domain of photolyases with its Rossmann-like fold in a distance of 17–18 Å to the catalytic FAD cofactor. In contrast to the deeply buried nucleotide-like antenna, the pterin derivative MTHF is bound close to the protein surface along the interface of the N- and C-terminal domains (20).

Like MTHF, the riboflavin derivatives FAD, FMN, as well as the riboflavin biosynthesis intermediate 6,7-dimethyl-8-ribityl-lumazin are commonly found in archaea, bacteria, and eukaryotes, whereas the occurrence of deazaflavin cofactors such as 8-HDF is more limited. For example, deazaflavins are signature molecules of methanogenic archaea, where 8-HDF in its oligoglutamylated and protonated F420 form plays an important role as a low potential hydride carrier (21). Nevertheless, deazaflavins are also found in several other bacterial clades such as the actinobacteria (22) as well as in unicellular green algae. The biological role of 8-HDF in photolyases was demonstrated in the green algae *Chlamydomonas reinhardtii*. Here, inactivation of the gene for the deazaflavin synthase PHR1 caused a loss of the photorepair of UV lesions as catalyzed in *C. reinhardtii* by the class II photolyase PHR2 (23). Interestingly, the (6-4) and class II CPD photolyases from the insect *Drosophila melanogaster* utilize 8-HDF as antenna chromophore as well (15), although this organism misses like other animals a genomic copy of the deazaflavin synthase gene. Instead, the bacterial symbiont *Wolbachia* was suggested to supply 8-HDF as a vitamin essential for photolyase function (14).

Here, we investigate the antenna chromophore of the class II CPD photolyase from *Methanosarcina mazei* (*Mm*CPDII) and the spectroscopic and structural characterization of its complex with the 8-HDF antenna. Together with phylogenetic data the structure of the *Mm*CPDII·8-HDF complex and its differences from higher plant photolyases allow us to predict the occurrence of 8-HDF in the whole metazoan branch of life.

EXPERIMENTAL PROCEDURES

Cloning of Streptomyces coelicolor FO Synthase—The gene *SCO4429* (*fbiC*) encoding the FO synthase (7,8-didemethyl-8-hydroxy-5-deazariboflavin synthase) of *Streptomyces coelicolor* (UniProt entry Q9KZZ7) was amplified from genomic DNA using the Phusion® DNA polymerase (Finnzymes) with primers 5′-GCATTGAATTCG**ATG**ACGACTTCCGCGACCTCC-3′ and 5′-GATATTCTCGAG**TTA**GTCCAGGACCGGCAGCAG-3′ (Metabion). The PCR product was cloned into pCR®2.1-TOPO® vector (Invitrogen) and subcloned via EcoRI

and XhoI sites (underlined) into pCDFDuet-1 (Novagen) thus yielding the cofactor plasmid pCDFDuet-His$_6$*Sc*FbiC, which encodes an N-terminally His$_6$-tagged *Sc*FbiC fusion.

Cloning of Photolyases for Co-expression Studies—The gene *Synpcc7942_0112* encoding the class I CPD photolyase (UniProt entry Q31S25) of *Synechococcus elongatus* PCC 7942 (*Anacystis nidulans* R2) was amplified from isolated genomic DNA with primers 5′-GGTTTGCAT**ATG**GCGGCTCCGATTCTGTTTTGG-3′ and 5′-CCAAACTCGAG**CTA**TGAATCGGGCTCAGCCTC-3′, thus introducing restriction sites for NdeI and XhoI (underlined). Accordingly, the PCR product was cloned into expression vector pET-28a (Novagen) to give the plasmid pET28a-His$_6$*An*CPDI. The latter encodes N-terminally His$_6$-tagged *An*CPDI. Likewise, the gene fragment (bases 1–1560) coding for the (6-4) photolyase domain from *D. melanogaster* (UniProt entry Q0E8P0) was amplified from the pDEST007 plasmid (9) with primers 5′-GCTTCGCAT**ATG**GATTCACAAAGGTCCACG-3′ and 5′-GCCCGTCTCGAG**TCA**GGTTTCTGATTTCTC-3′ and subcloned via NdeI and XhoI sites into pET-28a to produce pET-28a-His$_6$*Dm*(6-4). The class I CPD photolyase from *T. thermophilus* HB8 (UniProt entry P61497) was amplified from genomic DNA with primers 5′-GGAATTCCAT**ATG**GGCCCCCTTCTCGTC-3′ and 5′-CGCGGATCC**CTA**CCCTCGGGCGAGATCC-3′ (Invitrogen) and subcloned via NdeI and BamHI into pET-28a to yield pET-28aHis$_6$*Tt*CPDI.

Co-expression and Purification of Photolyases (PHR)—Escherichia coli BL21 (DE3) Gold cells (Stratagene) were transformed with either pET28a-His$_6$*Mm*CPDII (8), pET28a-His$_6$*An*CPDI, pET28a-His$_6$*Dm*(6-4), pET28a-His$_6$*Tt*CPDI, or pET28a-His$_6$*At*CPDII and the cofactor plasmid pCDFDuet-His$_6$*Sc*FbiC. Autoinduction-triggered co-expression was performed in terrific broth medium at 25 °C (*Mm*CPDII, *Tt*CPDI, *At*CPDII), 21 °C (*An*CPDI), and 18 °C (*Dm*(6-4)), respectively. Apart from *At*CPDII the putative photolyase·8-HDF complexes were purified according to the protocol of apo*Mm*CPDII apart that cell disruption was performed with a French press. For the purification of *At*CPDII buffer AT$_I$ (50 mM NaH_2PO_4, 500 mM NaCl, 20% (v/v) glycerol, pH 7.4) was used for affinity chromatography, and elution was performed by addition of 75 mM imidazole. Size exclusion chromatography was done in buffer AT$_{II}$ (20 mM Tris-HCl, 300 mM NaCl, 10% (v/v) glycerol, pH 7.4). The His$_6$-tagged FO synthase was efficiently removed by the size exclusion chromatography step.

Generation and Preparation of MmCPDII Mutants—Photolyase mutants *Mm*CPDII-S26L and *Mm*CPDII-S26F were obtained from pET28a-*Mm*CPDII by site-directed mutagenesis (QuikChange II; Agilent); resulting plasmids were verified by dideoxy-sequencing (Qiagen). Co-expression and purification of the Ser^{26} mutants were performed as described for the wild type photolyase.

In Vitro Reconstitution of ApoMmCPDII with Antenna Chromophores—Apo*Mm*CPDII (53 μM) was mixed with the equimolar amount of either FAD, FMN, MTHF, F420, or chemically synthesized 8-HDF. Afterward, all mixtures as well as negative controls were dialyzed at 4 °C against 1.5 ml of buffer I (10 mM Tris-HCl, 100 mM NaCl, pH 8.0) in a pre-greased VDX^{TM} plate (Hampton Research) using 10-μl microdialysis rods (Hampton Research) and a 3.5-kDa cutoff SnakeSkin® dialysis membranes (Pierce). After 24 h, reconstitution was analyzed by UV/visible spectroscopy using a NanoDrop 1000 spectrophotometer (Thermo Scientific). Likewise, the 8-HDF reference spectrum was recorded with the NanoDrop 1000 spectrophotometer and normalized to the *Mm*CPDII concentration used before.

TABLE 1
Crystallographic statistics of the *Mm*CPDII·8-HDF complexes
Values in parentheses denote the highest resolution shell.

	*Mm*CPDII·8-HDF$_{soak}$ (4CDM)	*Mm*CPDII·8-HDF (4CDN)
Data collection		
X-ray source	ID23-2	ID23-1
	ESRF, Grenoble, France	
Detector	MarCCD 225	ADSC Q315r
Wavelength (Å)	0.87260	0.97625
Space group	$P4_32_12$	$P2_12_12_1$
Cell dimensions (*a*,*b*,*c* Å)	69.89, 69.89, 245.5	78.97, 114.7, 141.4
Resolution (Å)	30.0-2.70 (2.85-2.70)	35.0-1.90 (2.00-1.90)
Total reflections	64,763	407,726
Multiplicity	4.2 (2.9)	4.1 (4.1)
Unique reflections	15,494	99,823
Completeness (%)	89.3 (84.9)	98.5 (98.7)
R_{merge} (%)	9.0 (32.0)	4.5 (43.3)
$I/\sigma(I)$	14.7 (4.5)	23.3 (3.2)
Mosaicity (°)	0.166	0.175
Wilson *B*-factor (Å^2)	38.3	25.6
Refinement		
Resolution (Å)	29.2-2.70	34.5-1.90
R_{factor}, R_{free}	0.206, 0.270	0.149, 0.178
Reflections (working, test set)	15,081, 216	97726, 2,022
Completeness for range (%)	88.1	98.1
r.m.s.d.[a] from ideal:		
Bond lengths (Å)	0.010	0.009
Bond angles (°)	1.278	1.354
Total number of atoms	3,826	8,267
Mean *B*-value (Å^2)	24.6	30.1

[a] r.m.s.d., root mean square deviation.

*Structure Determination of ApoMmCPDII Crystals Soaked with 8-HDF—Mm*CPDII crystals grown in 0.5 M lithium sulfate and 7.5% PEG 8000 were soaked for 30 min in crystallization buffer supplemented with 100 μM synthetic 8-HDF. During soaking changes in the integrity of *Mm*CPDII crystals were observed and are most likely reflected by the lower resolution limit of 2.7 Å compared with apo*Mm*CPDII crystals (1.5 Å). Before flash-freezing in liquid nitrogen crystals were soaked in the crystallization solution supplemented with 30% glycerol as cryoprotectant. Diffraction data were collected from a single crystal at 100 K at beamline ID23-2, European Synchrotron Radiation Facility (ESRF). Data processing was carried out using XDS and XSCALE (24) and further refinement using COOT (25) and REFMAC5 (26) at 2.7 Å resolution led to *R*-factors of R_{work} = 20.6% and R_{free} = 27.0%. Data processing and refinement statistics are summarized in Table l.

Crystallization and Structure Determination of the MmCPDII·8-HDF Complex—An initial 96-well format crystallization screening was performed with a Cartesian robot system and commercially available crystallization screens (Qiagen) using the sitting drop vapor diffusion method at 18 °C. First crystals were obtained in a crystallization condition containing 0.1 M lithium sulfate, 0.1 M trisodium citrate, pH 5.6, and 12% PEG 6000 within 48 h. Using the hanging drop vapor diffusion method and this condition, crystals suitable for data collection were grown in a 24-well plate at a protein concentration of 11.8

mg/ml. For cryoprotection, glycerol was added to a final concentration of 33%, and *Mm*CPDII·8-HDF crystals were flash-frozen in liquid nitrogen. X-ray data were collected from a single crystal at 100 K at beamline ID23-1, ESRF. *Mm*CPDII·8-HDF crystallized in the orthorhombic space group $P2_12_12_1$ with unit cell parameters $a = 78.97$ Å, $b = 114.7$ Å, $c = 141.4$ Å. Diffraction data were processed using XDS and XSCALE (24), and initial phases were obtained by molecular replacement using PHASER (27) and the structure of *Mm*CPDII in a tetragonal crystal form (2XRY) as search model. The correct solution with data up to 2.5 Å had two molecules per asymmetric unit with *z* scores of 25.7 for rotation and 45.9 for translation function for the first molecule and *z* scores of 26.2 and 79.7 for the second molecule, respectively. After initial automated model building from experimental phases as done by ARP/wARP (28), further refinement using COOT (25) and REFMAC5 (26) at 1.9 Å resolution led to *R*-factors of $R_{work} = 14.9\%$ and $R_{free} = 17.8\%$. Data processing and refinement statistics are summarized in Table 1. The nomenclature for the secondary structure of *Mm*CPDII is taken from Kiontke *et al.* (8). Structural analysis and figures were done with PyMOL 1.5 (29).

UV/Visible and Fluorescence Spectroscopy—UV/visible spectra were recorded using a V-660 spectrometer (JASCO) at 8 °C. Fluorescence spectroscopy of *Mm*CPDII in the oxidized state was carried out at 4 °C on a FP-6500 spectrofluorometer (Jasco). Samples of apo*Mm*CPDII and *Mm*CPDII·8-HDF with concentrations of 10 μM or 5.8 μM in buffer I were excited at a wavelength of 420 nm with band widths of 3 nm for excitation and 5 nm for emission, respectively. Reference fluorescence emission spectra were recorded with a high power LED (Roithner Lasertechnik), Maya 2000 Pro spectrometer (Ocean Optics) and SpectraSuite software (Ocean Optics). To generate the reduced state, samples of 16 μM *Mm*CPDII in 10 mM DTT were deoxygenized before being photoreduced on ice by illumination at 450 °nm for 10 min using a 450 °nm high power LED (Roithner Lasertechnik, 0.24 W/cm^2). Fluorescence emission/excitation spectra were recorded at 4 °C on a Fluorolog-3 (Horiba) using slit widths of 2 nm.

RESULTS AND DISCUSSION

In Vitro Reconstitution of MmCPDII with Synthetic 8-HDF—When purified via the *E. coli* expression system, recombinant class II photolyase from *M. mazei* (*Mm*CPDII) possesses the catalytic FAD cofactor but lacks any bound and host-derived antenna chromophore as shown before by UV/visible spectroscopy and structural analysis (8). To identify the cognate light-harvesting prosthetic group of *Mm*CPDII, we performed *in vitro* reconstitution of this so called apo*Mm*CPDII with known antenna chromophores such as FAD, FMN, MTHF, 8-HDF, and F420. Only for synthetic 8-HDF, the UV/visible spectroscopic analysis reveals a characteristically modified absorbance spectrum of the *M. mazei* class II photolyase. The absorbance spectrum of oxidized apo*Mm*CPDII with peaks at 362, 377, 421, 444, and 469 nm is dominated in the reconstituted *Mm*CPDII·8-HDF complex by a significant peak at 435 nm (Fig. 1). Furthermore, incorporation of deprotonated 8-HDF (λ_{max} 420 nm) into *Mm*CPDII causes a 15-nm red shift of the chromophore absorbance. This red shift of bound 8-HDF complies well with data reported for *D. melanogaster* (6-4) photolyase (14) and *A. nidulans* class I photolyase (*An*CPDI), the latter either purified directly from *A. nidulans* cells (16) or *in vitro* reconstituted with 8-HDF using recombinant enzyme (30, 31).

In Vivo Assembly of the MmCPDII·8-HDF Holoenzyme—To confirm these results and to rule out that incorporation of synthetic 8-HDF during *in vitro* reconstitution and crystal soaking is enforced by the chosen experimental conditions, an *in vivo* reconstitution system of *Mm*CPDII with endogenously produced 8-HDF was established. For this purpose, a cofactor plasmid encoding the *S. coelicolor* FO synthase (*Sc*FbiC), a bifunctional, *S*-adenosylmethionine-dependent enzyme (26), was constructed that enables the biosynthesis of 8-HDF in *E. coli* from 4-hydroxypyruvate and 5-amino-6-ribityl-amino-2,4(1*H*,3*H*)-pyrimidinedione, an intermediate of the riboflavin synthesis pathway (Fig. 2*A*). After nickel-nitrilotriacetic acid affinity chromatography, the *Mm*CPDII·8-HDF complex was separated from *Sc*FbiC by size exclusion chromatography (Fig. 2*B*). Like *in vitro* reconstituted *Mm*CPDII, the UV/visible spectrum of the *Mm*CPDII·8-HDF holoenzyme in the oxidized state is hallmarked by the distinct absorption maximum at 435 nm (Fig. 2*C*, *black line*) indicating that 8-HDF is bound to the photolyase. Moreover, the fluorescence emission spectrum of the complex exhibits a strong fluorescence peak at λ_{em} 467 nm (Fig. 2*C*, *thick red line*) and differs significantly from apo*Mm*CPDII with the latter exhibiting only broader emission at λ_{em} of approximately 528 nm for the oxidized FAD cofactor (Fig. 2*C*, *dotted red line*). In accordance with data from *An*CPDI (16, 31) and *Dm*(6-4) (14), the fluorescence maximum of *Mm*CPDII-bound 8-hydroxydeazaflavin resembles the maximum of deprotonated 8-HDF in solution with its λ_{em} of 470 nm (Fig. 3*A*). In contrast, the fully reduced $FADH^-$ state exhibits an emission peak for the 8-HDF antenna that is blue-shifted by 12 nm to 455 nm, thus suggesting some interaction between the redox state of the FAD cofactor and the structure of the antenna binding site (Fig. 2*D*). Furthermore, excitation spectra recorded at $\lambda_{em} = 533$ nm, the emission maximum of the reduced $FADH^-$ chromophore, demonstrate efficient Förster energy transfer between the antenna and the flavin cofactor, as the resulting spectra are clearly dominated by the 8-HDF antenna with its λ_{max} of 435 nm (Fig. 2*D*).

To clear up the question, whether Methanosarcinales are generally capable of synthesizing 8-HDF as cognate antenna of their photolyases, we performed a protein-protein BLAST search with *Methanocaldococcus jannaschii* CofG and CofH, which have been used before to produce artificial 8-HDF in *E. coli* (32). Indeed, *M. mazei* harbors like other methanosarcinal species, *e.g. Methanosarcina acetivorans* or *Methanosarcina barkeri*, one CofG and two CofH orthologues (SwissProt entries COFG_METMA, COFH1_METMA, COFH2_METMA).

Validation of the Heterologous in Vivo 8-HDF Reconstitution System—To rule out that our *in vivo* reconstitution system generates noncognate antenna-photolyase hybrids, class I and (6-4) photolyases were co-expressed with the *Sc*FbiC FO synthase. *An*CPDI was chosen as reliable positive control for successful incorporation of the 8-HDF antenna chromophore, because *An*CPDI that is directly purified from *A. nidulans* cells harbors 8-HDF as cognate antenna (16). This cyanobacterium

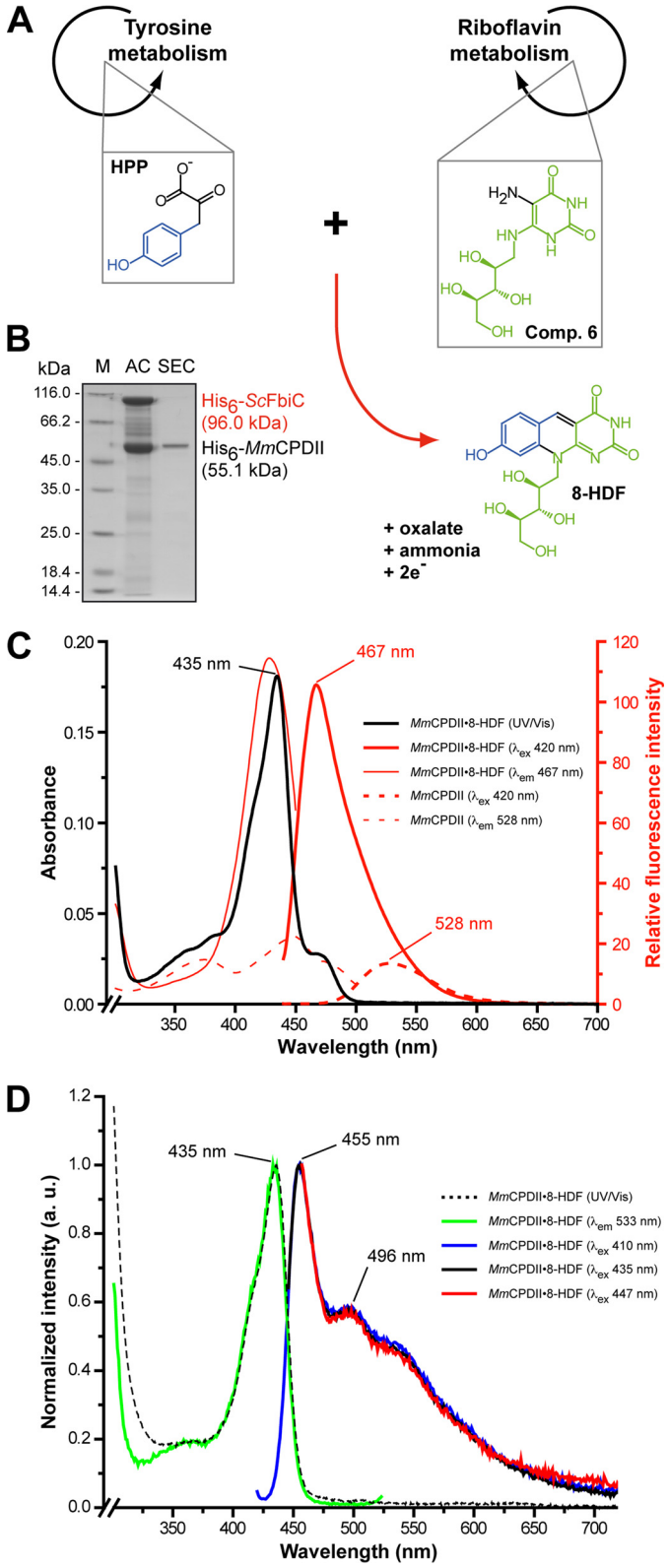

FIGURE 2. ***In vivo* reconstitution of *Mm*CPDII with an 8-HDF antenna prosthetic group.** *A*, the heterologous synthesis of 8-HDF in *E. coli* as catalyzed by the *S. coelicolor* FO synthase (*Sc*FbiC) starting from endogenous metabolites (4-hydroxyphenylpyruvate, compound 6: 5-amino-6-ribityl-amino-2,4(1*H*,3*H*)-pyrimidinedione). The reaction mechanism is according to Graham *et al.* (32). *B*, SDS-PAGE analysis showing the purification of the *Mm*CPDII·8-HDF complex. *C*, spectral properties of *Mm*CPDII and its complex with 8-HDF in the oxidized state. The UV/visible spectrum of the *Mm*CPDII·8-HDF complex (*black line*) features the identical absorbance maximum as the *in vitro* reconstituted photolyase. Unlike apo*Mm*CPDII (λ_{ex} 420 nm, *dotted red line*), the *Mm*CPDII·8-HDF complex features a prominent fluorescence emission maximum at 467 nm (λ_{ex} 420 nm, *solid red line*). The λ_{max} of 428 nm for the excitation spectrum of the *Mm*CPDII·8-HDF complex (emission measured at 467 nm, *thin red line*) indicates a bathochromic shift by about 8 nm for the absorption of the antenna chromophore due to its interactions with the photolyase. *D*, spectral properties of *Mm*CPDII and its complex with 8-HDF in the fully reduced state. The fluorescence excitation spectrum at 533 nm emission corresponds to 90% of the intensity when recorded at the emission maximum of the 8-HDF antenna of 455 nm.

carries genomic copies of the 8-HDF synthase genes *cofG* and *cofH* (UniProt entries Q5N4D1, Q5N3T7), on which biosynthesis of the 8-HDF chromophore depends. For comparison, the (6-4) photolyase from *D. melanogaster* as well as the class I CPD photolyase from *T. thermophilus* (*Tt*CPDI) were used, as the corresponding organisms lacking CofG/CofH orthologues. Here, 8-HDF has been successfully incorporated by either *in vitro* reconstitution of *Ds*(6-4) (14) or crystal soaking of *Tt*CPDI (33).

After purification, all putative recombinant photolyase complexes were analyzed by UV/visible spectroscopy to analyze for *in vivo* reconstitution with endogenously produced 8-HDF. In case of *An*CPDI and *Dm*(6-4) the UV/visible spectra exhibit prominent absorbance maxima at approximately 440–450 nm (Fig. 3*B*). Whereas the absorbance maximum of the *An*CPDI·8-HDF complex at λ_{max} 438 nm corresponds closely to spectra already published (16, 30, 31), the maximum at λ_{max} 448 nm for the *in vivo* reconstituted *Dm*(6-4)·8-HDF complex is red-shifted by 8 nm compared with the *in vitro* reconstituted photolyase with a λ_{max} of 440 nm (14). Interestingly, *in vivo* reconstitution with 8-HDF failed for *Tt*CPDI, although the FO synthase was solubly expressed (Fig. 3, *A*–*C*). Accordingly, the co-crystal structure of *Tt*CPDI with synthetic 8-HDF, which was generated by soaking *Tt*CPDI crystals with millimolar concentrations of 8-HDF (33), corresponds to a noncognate complex of this photolyase. However, the lack of endogenous 8-HDF biosynthesis pathways is not *per se* an indicator for 8-HDF playing no role as a cognate antenna chromophore of the respective photolyase. The fruit fly *D. melanogaster* lacks the genes required for 8-HDF biosynthesis, but its (6-4) and CPD photolyases are nevertheless capable of accommodating 8-HDF as antenna chromophore (15). This insect species may derive 8-HDF from a bacterial, hitherto unknown commensal as suggested before (14).

Structures of the MmCPDII·8-HDF Holoenzyme—To characterize 8-HDF antenna binding by *Mm*CPDII we derived co-crystal structures either by crystallization of *in vivo* reconstituted *Mm*CPDII·8-HDF holoenzyme at 1.9 Å resolution or by soaking apo*Mm*CPDII crystals with 8-HDF and subsequent structural analysis at 2.7 Å resolution. Interestingly, the holoenzyme crystallized in a novel, orthorhombic crystal form with two molecules per asymmetric symmetry unit (Table 1). Apart from differences in the linker region between the N- and C-terminal domain (Val^{186}-Glu^{231}) and the antenna binding loop there are almost no deviations between the *Mm*CPDII·8-HDF and the apo*Mm*CPDII structures. Furthermore, the root mean square deviations for complexes A and B of the *Mm*CPDII·8-HDF holoenzyme are low with 0.20 and 0.28 Å (330, 353 C_α atoms), respectively, relative to the apo*Mm*CPDII structure. In both reconstitutions, the 8-HDF chromophore is buried deeply

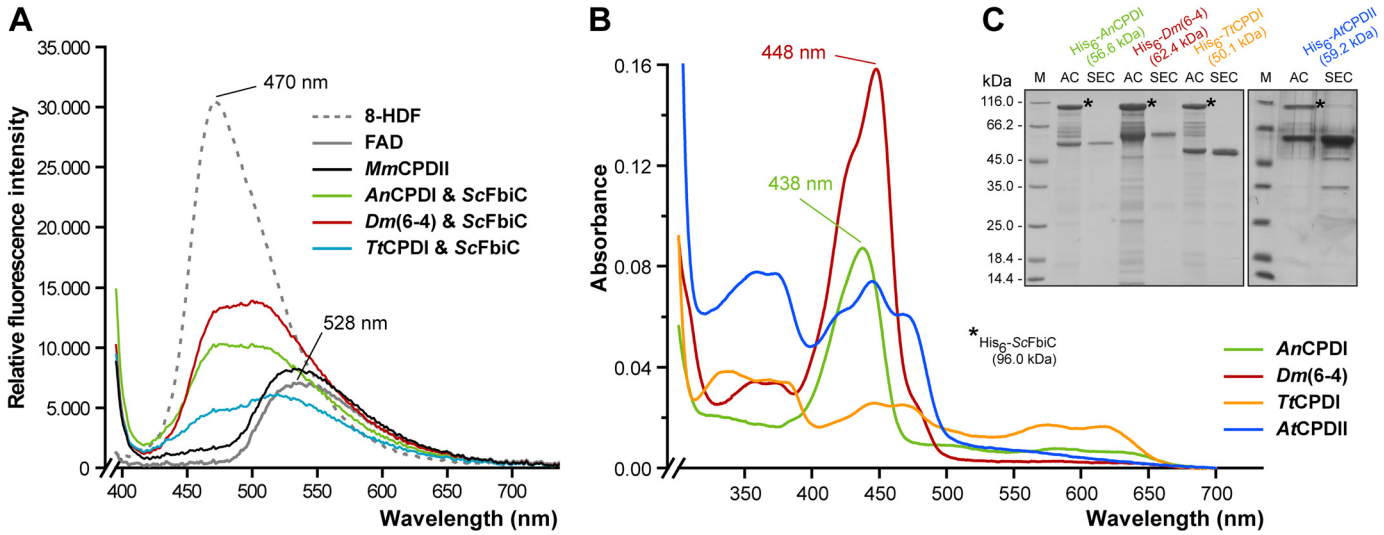

FIGURE 3. ***In vivo* reconstitution of different photolyases with 8-HDF.** *A*, fluorescence emission spectra of cofactor extracts from *E. coli* strains, which express different heterologous photolyases, as obtained by heat denaturation of endogenous proteins (λ_{ex} 385 nm). For comparison, *Mm*CPDII has been expressed in *E. coli* without a *Sc*FbiC transgene and shows accordingly only endogenous FAD fluorescence. Reference spectra for FAD (*solid*) and 8-HDF (*dotted*) are shown in *gray*. 3-fold averaged emission spectra were smoothed over three points. *B*, UV/visible spectra of purified *A. nidulans* class I CPD photolyase (*An*CPDI, *green line*) and *D. melanogaster* (6-4) photolyase (*Dm*(6-4), *red line*) showing absorbance maxima at 438 nm or 448 nm, respectively, which indicate bound 8-HDF, whereas the class II CPD photolyase from *A. thaliana* (*At*CPDII, *blue line*) fails to bind 8-HDF as antenna chromophore. Unlike previous results relying solely on crystal soaking (10), the *T. thermophilus* class I CPD photolyase (*Tt*CPDI, *orange line*) fails to incorporate 8-HDF. *C*, SDS-PAGE analysis of photolyase/*Sc*FbiC co-expressions. The *asterisks* mark the bands for the recombinant, co-expressed His_6-*Sc*FbiC. *M*, protein marker; *AC*, nickel-nitrilotriacetic acid affinity chromatography; *SEC*, size exclusion chromatography.

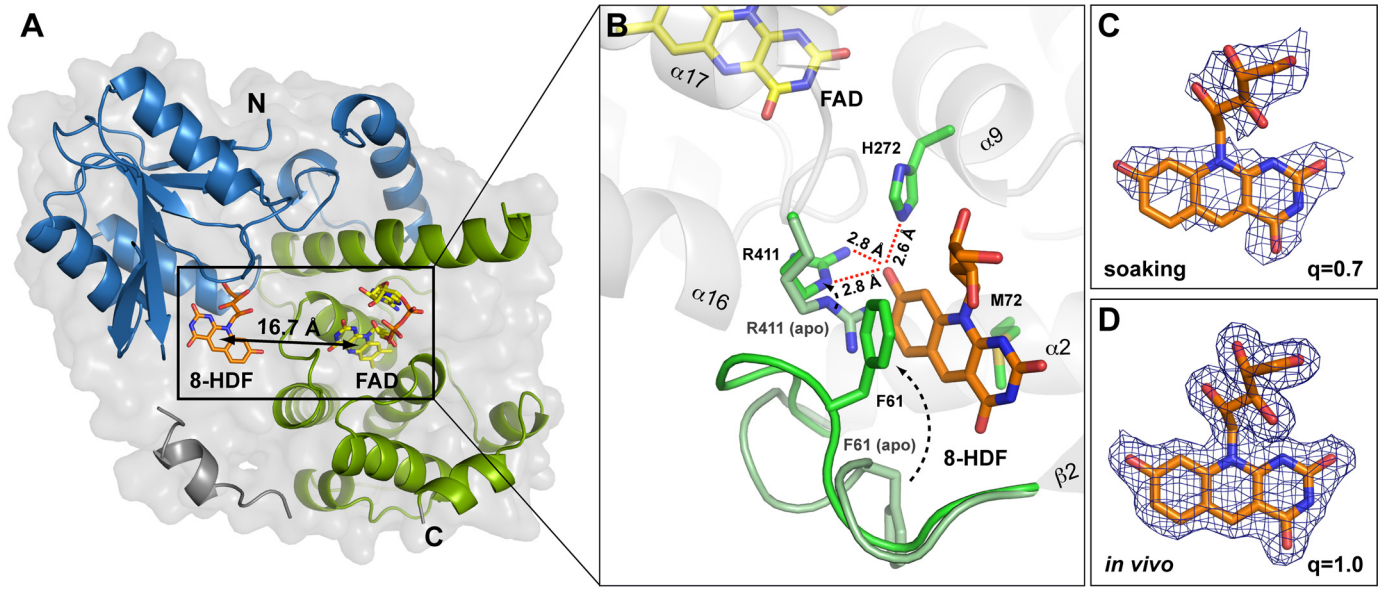

FIGURE 4. **Structural analysis of the *Mm*CPDII·8-HDF holoenzyme.** *A*, cut-away view of the overall structure. The antenna chromophore 8-HDF is bound within the N-terminal α/β domain (*blue*) in a distance suitable for Förster energy transfer to he catalytic cofactor FAD. *B*, structural details of the antenna chromophore binding pocket. The binding of 8-HDF causes conformational changes in the chromophore environment between apo*Mm*CPDII (*pale green*) and *Mm*CPDII·8-HDF holoenzyme (*green*). Comparison of the 8-HDF occupancies (*q*) resulting from either crystal soaking (*C*) or *in vivo* reconstitution in *E. coli* (*D*) is shown. Sigma-A weighted $2F_{obs} - F_{calc}$ electron densities are contoured at 1σ.

within the N-terminal domain in a distance of 16.7 Å to the catalytic FAD cofactor, which is well in range for efficient Förster energy transfer (Fig. 4, *A* and *B*). According to difference electron density the *in vivo* reconstituted *Mm*CPDII·8-HDF holoenzyme shows quantitative incorporation of the 8-HDF chromophore, whereas soaking achieved under our conditions only 70% occupancy (Fig. 4, *C* and *D*). The inhomogeneity of the latter is reflected by the alternative conformations taken up by parts of the antenna loop (Leu^{57}-Ala^{64}) that links β-strand β2 with helix α2. Here, the short helical turn (Glu^{60}-Glu^{63}) that is found in 8-HDF-free *Mm*CPDII structures (PDB codes 2XRY and 2XRZ (8)) undergoes a conformational change by closing the entrance to the 8-HDF binding site. The largest change within the antenna loop is made by Phe^{61}-Leu^{62}, which swivel their packed side chains by a distance of over 12 Å to form π-π-interaction between Phe^{61} and the middle ring of the deazaflavin (Fig. 4*B*).

The *in vivo* reconstituted *Mm*CPDII·8-HDF holoenzyme shows even larger conformational changes compared with the apo-structures of *Mm*CPDII. The rearrangement of the

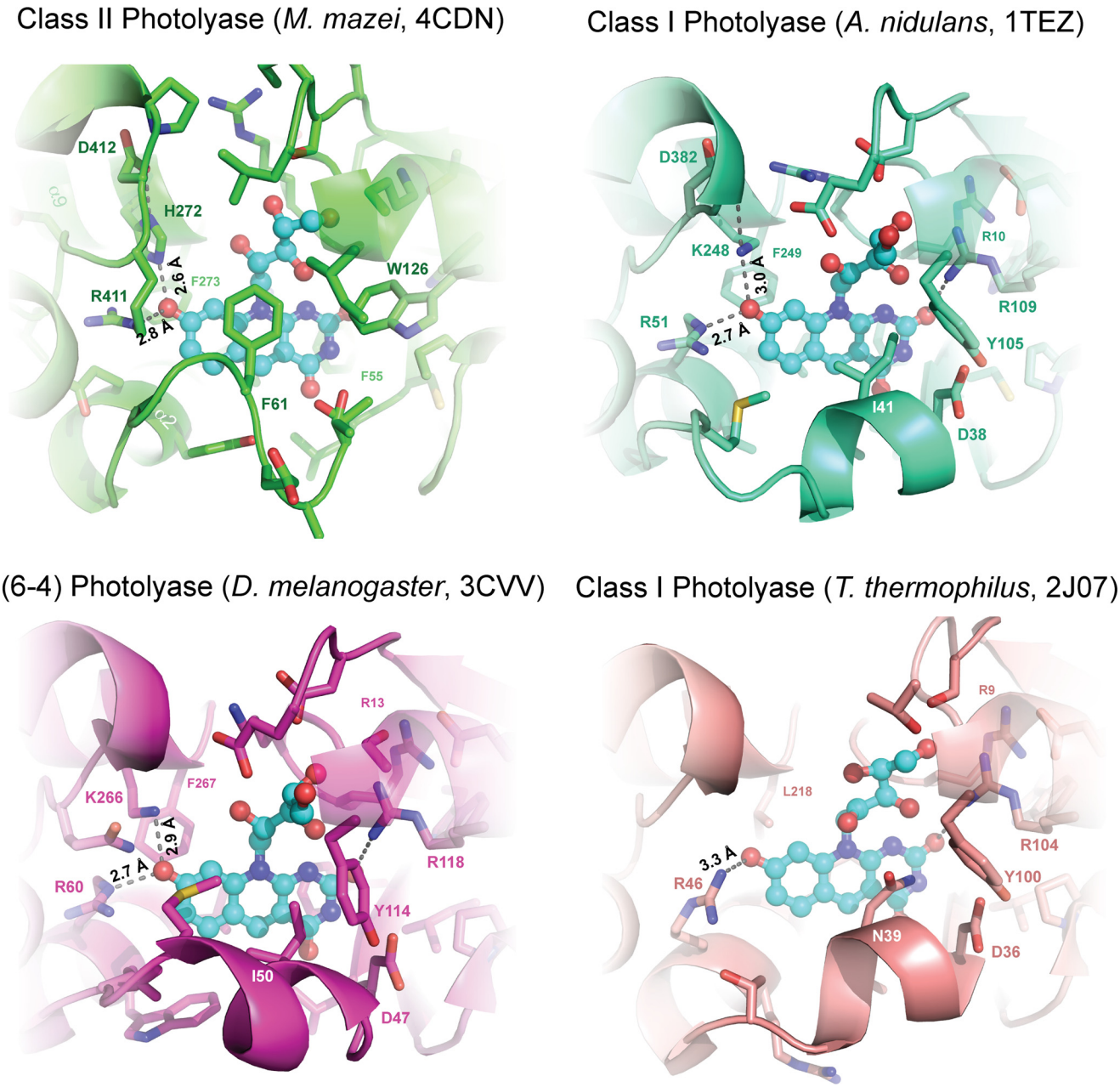

FIGURE 5. **Cognate and noncognate 8-HDF binding sites in the N-terminal antenna domain of DNA photolyases.** For clarity, the 8-HDF chromophore is shown as a *ball-and-stick* model.

antenna loop involves the region between Asp[59] and Ala[64] and seals the 8-HDF binding site from bulk solvent access. Furthermore, major parts of the linker between the N- and C-terminal domains of this photolyase (Val[186]-Glu[231]) either adopt a conformation different from in 8-HDF lacking *Mm*CPDII structures or are disordered as in complex B (Glu[189]-Leu[217]). In complex A, helix α7 (Leu[200]-Glu[214]), which is structurally also conserved in the class II photolyase from rice (*Oryza sativa*, PDB code 3UMV, Asp[221]-Glu[232] (11)), breaks down into three shorter helical segments (α7A, Leu[200]-Glu[205]; α7B, Val[208]-Leu[211]; α7C, Glu[214]-Lys[219]). The newly formed α7C segment hereby stabilizes the closed conformation of the antenna loop by several, newly formed van der Waal interactions. As a result Asp[222] of the linker that is exposed before as part of a loop becomes buried and forms a salt bridge with Arg[67]. Overall, these structural adaptations of the second shell around the antenna chromophore binding site most likely impede reopening and hence release of bound 8-HDF.

The Antenna Binding Site of MmCPDII—Although the 8-HDF chromophore locates in the same region of the N-terminal domain of *Mm*CPDII as in the cognate 8-HDF complexes of class I and (6-4) photolyases (Fig. 5), there are several peculiar differences for its binding site. First, the *re*-side of the aromatic ring system of 8-HDF, *i.e.* in Fig. 5 the backside, makes extensive van der Waal interactions with the bulky side chains of Phe[273] and Phe[55] as well as with Met[72] via its middle ring. In other photolyases, the latter residue is exchanged by a leucine, whereas the walling by phenylalanines is conserved. More

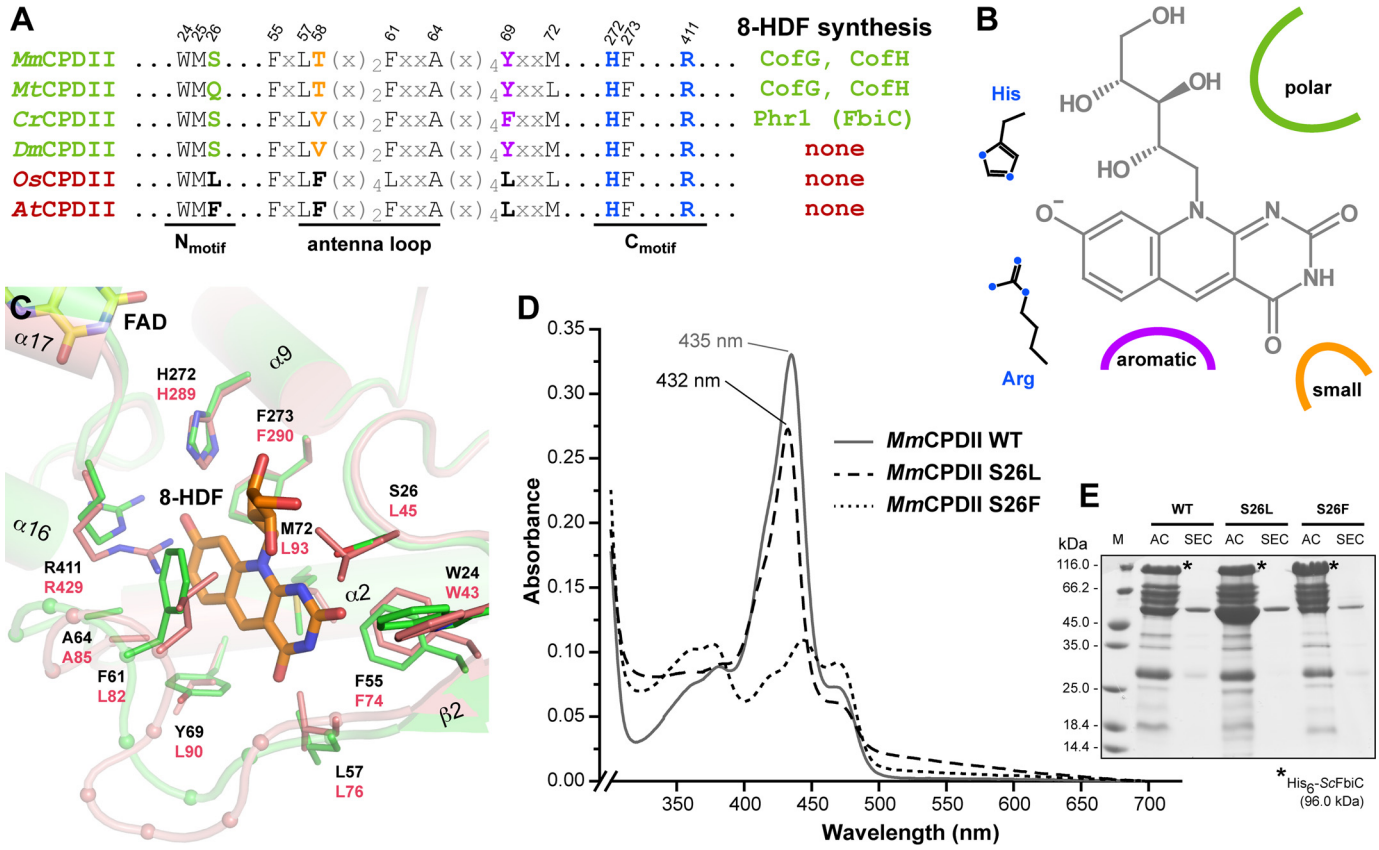

FIGURE 6. **Structural features of the 8-HDF binding pocket within class II photolyases.** *A*, the multiple sequence alignment of selected class II photolyases shows characteristic sequence motifs for 8-HDF binding like the N-motif presenting a polar side chain close to the ribityl moiety and the basic C-motif for salt bridge formation with 8-O^- group. *B*, schematic overview shows structural determinants of the 8-HDF binding motif. *C*, structural comparison of *Mm*CPDII (*green*) and *Os*CPDII (*rose*) identifies differences crucial for 8-HDF antenna chromophore binding. *D*, UV/visible spectroscopic analysis shows 8-HDF binding to *Mm*CPDII mutants. Replacement of the polar serine Ser^{26} within the WMS motif for a nonpolar leucine causes only a slight shift in the absorption maximum (*Mm*CPDII-S26L, *dashed line*), whereas the bulky, hydrophobic phenylalanine completely impeded 8-HDF incorporation (*Mm*CPDII-S26F, *dotted line*). *E*, SDS-PAGE analysis shows *Mm*CPDII mutant/*Sc*FbiC co-expressions. The *asterisks* mark the bands for the recombinant, co-expressed His_6-*Sc*FbiC. *M*, protein marker; *AC*, nickel-nitrilotriacetic acid affinity chromatography; *SEC*, size exclusion chromatography.

important, the *si*-side of the chromophore aromatic system is covered by Thr^{58} and Phe^{61} from the nonregular antenna loop, the indole of Trp^{126} as well as the side chain of Arg^{411}. In other photolyases, the antenna loop is replaced by a short helical segment, which points only with a leucine toward the middle ring of the 8-HDF chromophore. Second, Trp^{126} replaces in class II photolyases an otherwise highly conserved arginine residue (*An*CPDI, Arg^{109}; *Ds*(6-4), Arg^{118}), which forms in class I and (6-4) photolyases an H-bond to the C2-carbonyl of the deazaflavin moiety. In *Mm*CPDII, this role is taken by Ser^{26}, which forms hydrogen-bonds to the C2-carbonyl as well as the 3′-hydroxy group of the ribityl moiety (Fig. 5). Finally, two basic residues surround the phenolic ring of the 8-hydroxydeazaflavin to stabilize its deprotonated, anionic state. Only one of these residues, His^{272}, is similar in class I and 6-4 photolyases (*An*CPDI, Lys^{248}; *Ds*(6-4), Lys^{266}), where it forms a salt bridge to the 8-oxy group of 8-HDF. The conformation of this histidine is stabilized by a salt bridge to Asp^{412} from the C-terminal domain of *Mm*CPDII (Fig. 5). Interestingly, its preceding residue, Arg^{411}, makes the second salt bridge to the 8-oxy group. This residue has no counterpart in class I and (6-4) photolyases and is replaced in the latter by an arginine from the N-terminal domain (*An*CPDI, Arg^{51}; *Ds*(6-4), Arg^{60}).

Given other structural differences, which are crucial for function, *e.g.* the distinct electron-transfer pathways for photoreduction or the binding sites of the catalytic FAD chromophore (8), these observations corroborate the notion of a large evolutionary gap between class II photolyases and other members of the photolyase-cryptochrome superfamily. For example, class I photolyases that lack 8-HDF as cognate antenna such as *Tt*CPDI, miss all of the ascribed motifs of the 8-HDF binding site (Fig. 5).

Conservation of the 8-HDF Antenna Chromophore within Class II Photolyases—Apart from the structural differences described above, a comparison of the *Mm*CPDII·8-HDF complex and the recently published *O. sativa* class II CPD photolyase (*Os*CPDII) shows no other major deviations. Nevertheless, heterologously expressed *O. sativa* photolyase lacks any kind of an additional antenna chromophore as shown previously by UV/visible spectroscopy (34) as well as by current structural characterization (11). Likewise, the heterologously overexpressed class II photolyases from *Arabidopsis thaliana*, whose sequence identity to *Os*CPDII exceeds 65%, fails to incorporate under our *in vivo* conditions any 8-HDF chromophore (Fig. 3, *B* and *C*). A superimposition of the *Os*CPDII structure with the *Mm*CPDII·8-HDF complex (root mean

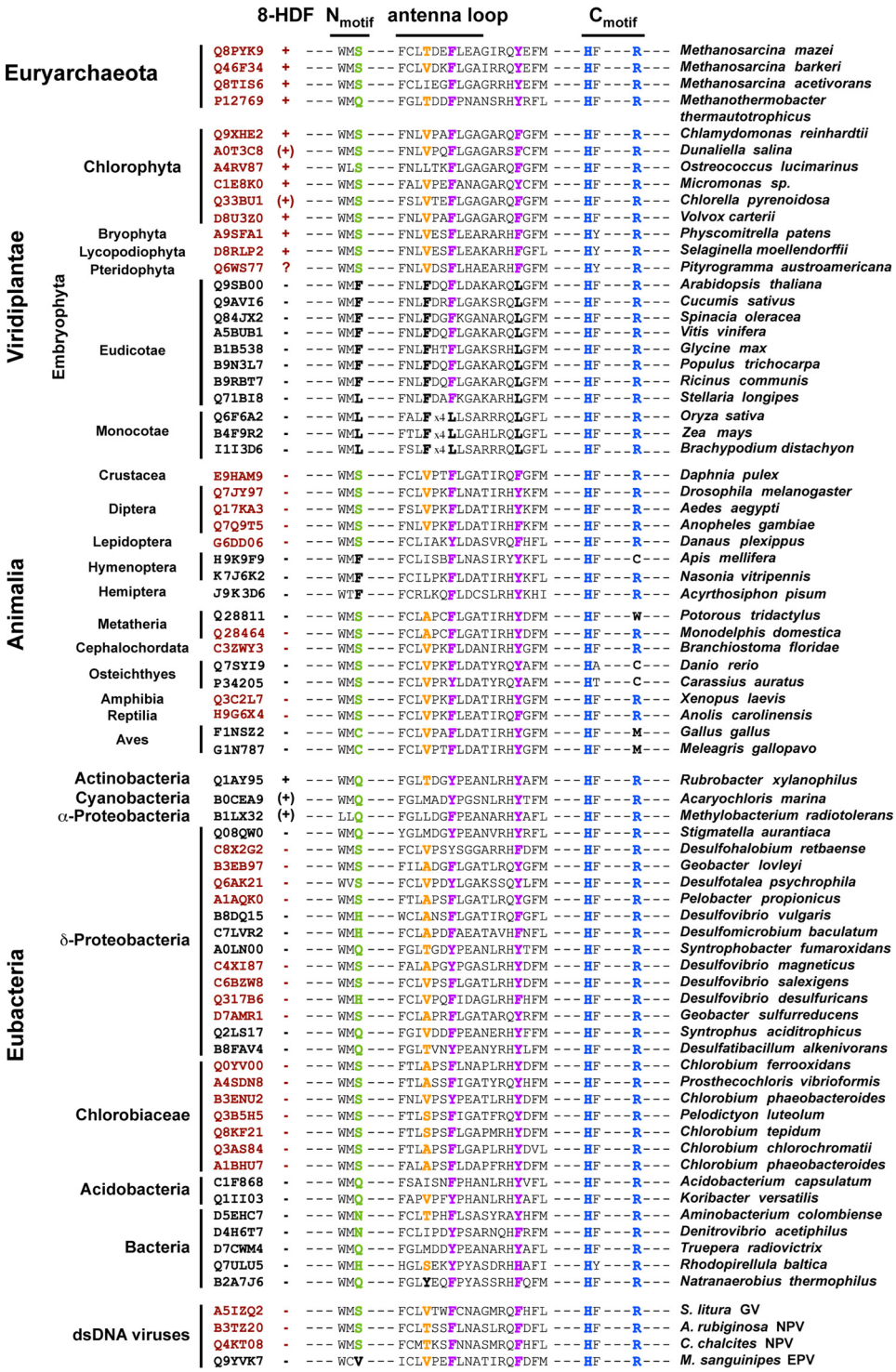

FIGURE 7. **Excerpt of a multiple sequence alignment for class II photolyases highlighting orthologues that participate in the formation of the 8-HDF binding site (shown in *red*; entry codes are listed in *left column*).** For comparison class II photolyases with binding sites, which are predicted to be incapacitated of 8-HDF binding, are highlighted in *black*. The column 8-HDF predicts the endogenous occurrence of the 5-deazaflavin chromophore according to the genomic encoding of 8-HDF synthase-like enzymes: +, yes; −, no; ?, unknown; (+) = 8-HDF synthase-like enzymes are present in the genus (*Chlorella*) and in the order (*D. salina*: Chlamydomonadales; *A. marina*: Chroococcales; *M. radiotolerans*: Rhizobiales), respectively. Further abbreviations: *GV*, granulovirus; *NPV*, nucleopolyhedrovirus; *EPV*, entomopoxvirus.

square deviation 0.60 Å for 338 Cα atoms) shows that although most amino acids lining the antenna binding pocket are either conserved (*Os*CPDII: Trp[43], Leu[76], Ala[85], His[289], Phe[290], Arg[429]) or have at least similar biochemical properties (see Fig. 6*C*). However, there are several peculiar differences correlating with the loss of 8-HDF binding. First, the "lower" part of the pocket, where the aromatic ring moiety of 8-HDF is accommodated, lacks in *Os*CPDII the aromatic residues from the antenna loop that are responsible for π-π stacking from the *si*-side (*Mm*CPDII, Phe[61]; *Os*CPDII, Leu[82]) as well as the edge-to-face

interaction with the Cys[6] of the deazaflavin (*Mm*CPDII, Tyr[69]; *Os*CPDII, Leu[90] (35)). Instead, the binding pocket is partly filled in *Os*CPDII by the bulky side chain of Phe[77] (*Mm*CPDII: Thr[58]) from the antenna loop. Second, in *Os*CPDII a leucine (Leu[45]) replaces the polar residue Ser[26] of *Mm*CPDII, which is crucial for the recognition of 8-HDF via the H-bonds to the C2-carbonyl and 3′-hydroxy group. In contrast, the basic residues His[272] and Arg[411] of the C-terminal catalytic domain, which stabilize the deprotonation of the 8-hydroxy group, are preserved in the higher plant photolyases like *At*CPDII or *Os*CPDII and are hence only weak indicators for antenna chromophore binding.

Taken together, we can now predict the signature motifs, by which members of the class II photolyase family are capable of utilizing 8-HDF as a cognate antenna (Fig. 6, *A* and *B*). First, the C-motif harboring the basic residues His[272] and Arg[411] has to be intact for interacting with the deprotonated 8-oxy group of 8-HDF. Second, the N-motif (WM**S**) has to provide a polar residue for H-bonding interactions with 8-HDF as well as formation of the binding site wall. A replacement of this residue by a bulky aromate like in the S26F mutant of *Mm*CPDII and predictably most plant eudicots is incompatible with 8-HDF antenna binding due to steric hindrance, whereas a smaller exchange by leucine is still tolerated for the *in vivo* incorporation of 8-HDF (Fig. 6, *D* and *E*). Third, a small nonbulky residue (*Mm*CPDII: Thr[58]) as well as the aromatic residues of the antenna loop are required for forming the binding site covering the *si*-side of the 8-HDF chromophore. Apart from the methanosarcinal photolyases, several bacterial class II photolyases fulfill these criteria such as those from *Rubrobacter xylanophilus* or members of the classes Chlorobiaceae and Desulfovibrionales. Interestingly, only a few of these microorganisms carry genes for a CofG orthologue for endogenous 8-HDF biosynthesis (Figs. 6*A* and 7), implying that many microbes may depend on the supply of 8-HDF from the environment for assembling antenna-bearing CPD photolyases. In the plant kingdom, green algae like *C. reinhardtii* or the *Ostreococcus* species own class II photolyases with cognate motifs for 8-HDF recognition together with genome-encoded deazaflavin synthases, *e.g.* PHR1 from *C. reinhardtii* (23). Interestingly, the ability to utilize 8-HDF antenna comprising class II photolyases for DNA repair is not restricted to these simple, still microbial model systems of higher plants, but is also maintained in land plants like mosses, lycophytes, and ferns. These embryophytes encode class II photolyases with intact 8-HDF binding sites as well as bifunctional CofG/CofH-like synthases for 8-HDF (*Physcomitrella patens*, A9SZ46; *Selaginella moellendorffii*, XP_002968233). Seed plants, *i.e.* angio- and gymnosperms, have apparently lost the ability to equip their class II photolyases with the deazaflavin antenna chromophore due to a loss of the corresponding 8-HDF synthases. Given the structural features at the antenna binding site of the monocot *Os*CPDII photolyase, where not only the region accommodating the pyrimidine ring is occupied by a leucine replacing Ser[26] of *Mm*CPDII, but also affected by a two residue longer antenna loop (Fig. 7), one may argue that the photolyases from monocots and eudicots are capable of recognizing other antenna chromophores than the known ones. For example, colored secondary metabolites such as isoflavonoids, aurones, and anthocyanins have only evolved in gymnosperms and angiosperms (36) and may replace the 8-HDF antenna of class II photolyases, which are predicted to be still present in fern and moss photolyases.

Interestingly, class II photolyases from animals present a more perplexing view. Clearly, all known animal genomes indicate the absence of any biosynthesis pathway for deazaflavins. Nevertheless, both the (6-4) as well as the CPD photolyases from the insect *D. melanogaster* can be reconstituted with an 8-HDF antenna (14, 15). Likewise, other diphtheria, *e.g.* the vectors for malaria and West Nile fever, *Anopheles gambiae* and *Aedes aegyptii*, encode class II photolyases compatible with 8-HDF antenna chromophores (Fig. 7). Interestingly, the earlier notion that endosymbiotic *Wolbachia* or *Spiroplasma* species may be the source of 8-HDF for *D. melanogaster* photolyases (14) is not supported by genomic data, which predict a lack of 8-HDF biosynthesis pathways in these bacteria. Accordingly, class II photolyases compatible with 8-HDF antennas are not a general trait in the insect class, because the class II photolyases from hemiptera and hymenoptera like the honey bee (*Apis mellifera*) show substitutions similar to those found in the higher plant photolyases. The same diversity also holds for the vertebrates. Here, many amphibians, reptilians, and even non-placental mammals encode 8-HDF utilizing class II photolyases (Fig. 7), whereas others like birds and bony fishes show substitutions in their photolyases genes, which ablate 8-HDF binding.

CONCLUSION

8-HDF is an apparently widespread antenna chromophore of photolyases not only among microbial organisms, but also in plants and animals. In the latter, it may fulfill a role as a vitamin as suggested before for the (6-4) photolyases from *D. melanogaster* (14). Suitable supplies for 8-HDF are many classes of gut microbes, *e.g.* methanosarcinales, or the environment. Given previous attempts to improve the UV resistance of mammals and plants by introducing photolyase transgenes into these organisms one can postulate that the provision of a suitable pathway for antenna chromophore biosynthesis may be a prerequisite as well.

Acknowledgments—We thank Annegret Wilde (Justus-Liebig University, Giessen) and Verena Helmetag (Philipps-University, Marburg) for genomic DNA, Elvira Happel and Emine Kaya (Ludwig-Maximilians University, Munich) for plasmids, Seigo Shima (Max-Planck Institute for Terrestrial Microbiology, Marburg) for a sample of F_{420}, and Christoph Schwarz, Dennis Walczyk, and Sophie Franz for technical assistance. Synthetic 8-HDF was a gift from Thomas Carell (Ludwig-Maximilians University, Munich). We thank the beamline staff of ID23-1 and ID23-2 at the European Synchrotron Radiation Facility (ESRF Grenoble, France) for excellent support during data collection.

REFERENCES

1. Essen, L. O. (2006) Photolyases and cryptochromes: common mechanisms of DNA repair and light-driven signaling? *Curr. Opin. Struct. Biol.* **16,** 51–59
2. Sancar, A. (2003) Structure and function of DNA photolyase and cryptochrome blue-light photoreceptors. *Chem. Rev.* **103,** 2203–2237

3. Kato, T., Jr., Todo, T., Ayaki, H., Ishizaki, K., Morita, T., Mitra, S., and Ikenaga, M. (1994) Cloning of a marsupial DNA photolyase gene and the lack of related nucleotide sequences in placental mammals. *Nucleic Acids Res.* **22,** 4119–4124
4. Lucas-Lledó, J. I., and Lynch, M. (2009) Evolution of mutation rates: phylogenomic analysis of the photolyase/cryptochrome family. *Mol. Biol. Evol.* **26,** 1143–1153
5. Müller, M., and Carell, T. (2009) Structural biology of DNA photolyases and cryptochromes. *Curr. Opin. Struct. Biol.* **19,** 277–285
6. Liu, Z., Tan, C., Guo, X., Kao, Y. T., Li, J., Wang, L., Sancar, A., and Zhong, D. (2011) Dynamics and mechanism of cyclobutane pyrimidine dimer repair by DNA photolyase. *Proc. Natl. Acad. Sci. U.S.A.* **108,** 14831–14836
7. Thiagarajan, V., Byrdin, M., Eker, A. P., Müller, P., and Brettel, K. (2011) Kinetics of cyclobutane thymine dimer splitting by DNA photolyase directly monitored in the UV. *Proc. Natl. Acad. Sci. U.S.A.* **108,** 9402–9407
8. Kiontke, S., Geisselbrecht, Y., Pokorny, R., Carell, T., Batschauer, A., and Essen, L. O. (2011) Crystal structures of an archaeal class II DNA photolyase and its complex with UV-damaged duplex DNA. *EMBO J.* **30,** 4437–4449
9. Maul, M. J., Barends, T. R., Glas, A. F., Cryle, M. J., Domratcheva, T., Schneider, S., Schlichting, I., and Carell, T. (2008) Crystal structure and mechanism of a DNA (6-4) photolyase. *Angew Chem. Int. Ed. Engl.* **47,** 10076–10080
10. Mees, A., Klar, T., Gnau, P., Hennecke, U., Eker, A. P., Carell, T., and Essen, L. O. (2004) Crystal structure of a photolyase bound to a CPD-like DNA lesion after *in situ* repair. *Science* **306,** 1789–1793
11. Hitomi, K., Arvai, A. S., Yamamoto, J., Hitomi, C., Teranishi, M., Hirouchi, T., Yamamoto, K., Iwai, S., Tainer, J. A., Hidema, J., and Getzoff, E. D. (2012) Eukaryotic class II cyclobutane pyrimidine dimer photolyase structure reveals basis for improved ultraviolet tolerance in plants. *J. Biol. Chem.* **287,** 12060–12069
12. Johnson, J. L., Hamm-Alvarez, S., Payne, G., Sancar, G. B., Rajagopalan, K. V., and Sancar, A. (1988) Identification of the second chromophore of *Escherichia coli* and yeast DNA photolyases as 5,10-methenyltetrahydrofolate. *Proc. Natl. Acad. Sci. U.S.A.* **85,** 2046–2050
13. Klar, T., Pokorny, R., Moldt, J., Batschauer, A., and Essen, L. O. (2007) Cryptochrome 3 from *Arabidopsis thaliana*: structural and functional analysis of its complex with a folate light antenna. *J. Mol. Biol.* **366,** 954–964
14. Glas, A. F., Maul, M. J., Cryle, M., Barends, T. R., Schneider, S., Kaya, E., Schlichting, I., and Carell, T. (2009) The archaeal cofactor F0 is a light-harvesting antenna chromophore in eukaryotes. *Proc. Natl. Acad. Sci. U.S.A.* **106,** 11540–11545
15. Selby, C. P., and Sancar, A. (2012) The second chromophore in *Drosophila* photolyase/cryptochrome family photoreceptors. *Biochemistry* **51,** 167–171
16. Eker, A. P., Kooiman, P., Hessels, J. K., and Yasui, A. (1990) DNA photoreactivating enzyme from the cyanobacterium *Anacystis nidulans*. *J. Biol. Chem.* **265,** 8009–8015
17. Ueda, T., Kato, A., Kuramitsu, S., Terasawa, H., and Shimada, I. (2005) Identification and characterization of a second chromophore of DNA photolyase from *Thermus thermophilus* HB27. *J. Biol. Chem.* **280,** 36237–36243
18. Fujihashi, M., Numoto, N., Kobayashi, Y., Mizushima, A., Tsujimura, M., Nakamura, A., Kawarabayasi, Y., and Miki, K. (2007) Crystal structure of archaeal photolyase from *Sulfolobus tokodaii* with two FAD molecules: implication of a novel light-harvesting cofactor. *J. Mol. Biol.* **365,** 903–910
19. Geisselbrecht, Y., Frühwirth, S., Schroeder, C., Pierik, A. J., Klug, G., and Essen, L. O. (2012) CryB from *Rhodobacter sphaeroides*: a unique class of cryptochromes with new cofactors. *EMBO Rep.* **13,** 223–229
20. Chaves, I., Pokorny, R., Byrdin, M., Hoang, N., Ritz, T., Brettel, K., Essen, L. O., van der Horst, G. T., Batschauer, A., and Ahmad, M. (2011) The cryptochromes: blue light photoreceptors in plants and animals. *Annu. Rev. Plant Biol.* **62,** 335–364
21. Walsh, C. (1986) Naturally occurring 5-deazaflavin coenzymes: biological redox roles. *Acc. Chem. Res.* **19,** 216–221
22. Isabelle, D., Simpson, D. R., and Daniels, L. (2002) Large-scale production of coenzyme F420–5,6 by using *Mycobacterium smegmatis*. *Appl. Environ. Microbiol.* **68,** 5750–5755
23. Petersen, J. L., and Small, G. D. (2001) A gene required for the novel activation of a class II DNA photolyase in *Chlamydomonas*. *Nucleic Acids Res.* **29,** 4472–4481
24. Kabsch, W. (1993) Automatic processing of rotation diffraction data from crystals of initially unknown symmetry and cell constants. *J. Appl. Crystallogr.* **26,** 795–800
25. Emsley, P., Lohkamp, B., Scott, W. G., and Cowtan, K. (2010) Features and development of COOT. *Acta Crystallogr. D Biol. Crystallogr.* **66,** 486–501
26. Murshudov, G. N., Vagin, A. A., and Dodson, E. J. (1997) Refinement of macromolecular structures by the maximum-likelihood method. *Acta Crystallogr. D Biol. Crystallogr.* **53,** 240–255
27. McCoy, A. J., Grosse-Kunstleve, R. W., Adams, P. D., Winn, M. D., Storoni, L. C., and Read, R. J. (2007) PHASER crystallographic software. *J. Appl. Crystallogr.* **40,** 658–674
28. Langer, G., Cohen, S. X., Lamzin, V. S., and Perrakis, A. (2008) Automated macromolecular model building for x-ray crystallography using ARP/wARP version 7. *Nat. Protoc.* **3,** 1171–1179
29. DeLano, W. L. (2002) *The PyMOL Molecular Graphics System*, DeLano Scientific, San Carlos, CA
30. Kort, R., Komori, H., Adachi, S., Miki, K., and Eker, A. (2004) DNA apophotolyase from *Anacystis nidulans*: 1.8 Å structure, 8-HDF reconstitution and x-ray-induced FAD reduction. *Acta Crystallogr. D Biol. Crystallogr* **60,** 1205–1213
31. Malhotra, K., Kim, S. T., Walsh, C., and Sancar, A. (1992) Roles of FAD and 8-hydroxy-5-deazaflavin chromophores in photoreactivation by *Anacystis nidulans* DNA photolyase. *J. Biol. Chem.* **267,** 15406–15411
32. Graham, D. E., Xu, H., and White, R. H. (2003) Identification of the 7,8-didemethyl-8-hydroxy-5-deazariboflavin synthase required for coenzyme F(420) biosynthesis. *Arch. Microbiol.* **180,** 455–464
33. Klar, T., Kaiser, G., Hennecke, U., Carell, T., Batschauer, A., and Essen, L. O. (2006) Natural and non-natural antenna chromophores in the DNA photolyase from *Thermus thermophilus*. *ChemBioChem* **7,** 1798–1806
34. Okafuji, A., Biskup, T., Hitomi, K., Getzoff, E. D., Kaiser, G., Batschauer, A., Bacher, A., Hidema, J., Teranishi, M., Yamamoto, K., Schleicher, E., and Weber, S. (2010) Light-induced activation of class II cyclobutane pyrimidine dimer photolyases. *DNA Repair* **9,** 495–505
35. Chakrabarti, P., and Bhattacharyya, R. (2007) Geometry of nonbonded interactions involving planar groups in proteins. *Progr. Biophys. Mol. Biol.* **95,** 83–137
36. Rausher, M. D. (2006) in *The Science of Flavonoids* (Grotewold, E., ed) pp. 175–211, Springer, New York